The Journal of Experimental Biology 211, 3478-3489
Published by The Company of Biologists 2008
doi:10.1242/jeb.017590

Kinematics of slow turn maneuvering in the fruit bat *Cynopterus brachyotis*

José Iriarte-Díaz[1,*] and Sharon M. Swartz[1,2]

[1]Department of Ecology and Evolutionary Biology and [2]Division of Engineering, Brown University, Providence, RI 02912, USA

*Author for correspondence at current address: Department of Organismal Biology and Anatomy, University of Chicago, Chicago, IL 60637, USA (e-mail: jiriarte@uchicago.edu)

Accepted 6 September 2008

SUMMARY

Maneuvering abilities have long been considered key factors that influence habitat selection and foraging strategies in bats. To date, however, very little experimental work has been carried out to understand the mechanisms that bats use to perform maneuvers. In the present study, we examined the kinematics of slow-speed turning flight in the lesser short-nosed fruit bat, *Cynopterus brachyotis*, to understand the basic mechanics employed to perform maneuvers and to compare them with previous findings in bats and other flying organisms. Four individuals were trained to fly in L-shaped flight enclosure that required them to make a 90 deg. turn midway through each flight. Flights were recorded with three low-light, high-speed videocameras, allowing the three-dimensional reconstruction of the body and wing kinematics. For any flying organisms, turning requires changes of the direction of travel and the reorientation of the body around the center of mass to maintain the alignment with the flight direction. In *C. brachyotis*, changes in body orientation (i.e. heading) took place during upstroke and preceded the changes in flight direction, which were restricted to the downstroke portion of the wingbeat cycle. Mean change in flight direction was significantly correlated to the mean heading angular velocity at the beginning of the downstroke and to the mean bank angle during downstroke, although only heading velocity was significant when both variables were considered. Body reorientation prior to changes in direction might be a mechanism to maintain the head and body aligned with the direction of travel and, thus, maximizing spatial accuracy in three-dimensionally complex environments.

Supplementary material available online at http://jeb.biologists.org/cgi/content/full/211/21/3478/DC1

Key words: aerodynamics, bat, flight, kinematics, turning.

INTRODUCTION

Flight maneuverability in bats is subject to strong selective pressures. Many bats inhabit and navigate rapidly through cluttered environments and the ability to perform quick and sharp changes in flight direction is likely to play an important role in their survival in natural environments. Accordingly, it has been hypothesized that variation in maneuvering performance strongly influences habitat selection and foraging strategies in bats (Norberg and Rayner, 1987). However, most studies of the morphological basis of bird and bat maneuvering have been restricted to analyses based on fixed-wing aerodynamics (Rayner and Aldridge, 1985; Aldridge, 1987; Warrick, 1998), even though flying animals turn using unsteady dynamics, violating the assumptions of steady-state aerodynamic theory. Although the degree to which assuming fixed-wing models introduces error in analysis is unknown, predictions derived from steady-state models have been applied extensively in the bird and bat research communities, particularly when looking for morphological correlates of flight performance and its ecological implications (e.g. Aldridge, 1986a; Norberg and Rayner, 1987; Kalcounis and Brigham, 1995). Recent information on maneuvering flight of birds (Warrick and Dial, 1998; Warrick et al., 1998; Hedrick and Biewener, 2007; Hedrick et al., 2007) and insects (Fry et al., 2003; Card and Dickinson, 2008) has expanded the discussion beyond the assumption of fixed wings. These studies emphasize the importance of temporal sequences of wing movements to understand the mechanical basis of turning behavior. Although bats are believed by some to be the most maneuverable flying animals for their size, no analogous studies have been performed for bats. In the present study, we evaluate the morphological and aerodynamic mechanisms used by bats to carry out 90 deg. turns at slow speed by analyzing wing and body kinematics in detail.

To successfully complete a turn, an animal must translate its center of mass (CoM) along the flight path (i.e. change its flight direction) and rotate its body around its CoM to align its body orientation with the new direction. The magnitude of change in direction of flight is a function of the impulse (force·time) perpendicular to the original direction of movement. Impulse is the result of the centripetal force produced by the change of the orientation of the net aerodynamic force generated by the body and wings. Two basic strategies to produce a turning force include banked and crabbed turns (Fig. 1). In a banked turn, the animal rolls around its cranio-caudal axis, tilting the vector of the vertical component of the net aerodynamic force (i.e. lift in level flight) laterally and towards the center of the turn (Fig. 1). These turns are used by most fixed-wing aircrafts (Filippone, 2006). By contrast, in a crabbed turn, the animal yaws into the turn, orienting the forward component of the net aerodynamic force (i.e. thrust in level flight) towards the center of the turn, without the need of adjusting the vertical component vector (Fig. 1). In both cases, the reorientation of aerodynamic forces produces a laterally oriented force that drives the organism into a turn. Both banked and crabbed turning mechanisms require the rotation of the body about its CoM.

Banked turns appear more common in animal flight. They have been described for organisms as diverse as fruit flies (Fry et al., 2003), locusts (Berger and Kutsch, 2003), dragonflies (Alexander, 1986), gliding frogs (McCay, 2001) gliding mammals (Bishop and

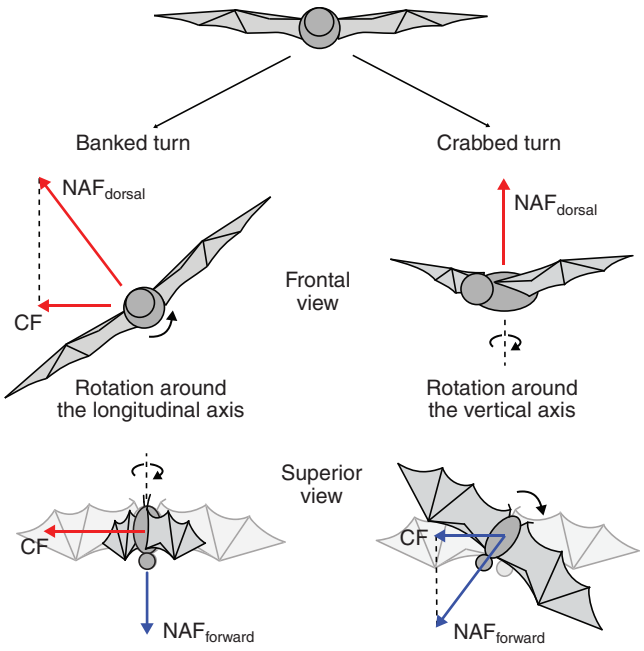

Fig. 1. Diagram showing two types of turning mechanisms. (A) A banked turn, in which a bat rolls into the turn. By banking the body, a bat tilts the dorsal component of the net aerodynamic force (NAF_{dorsal}) produced during downstroke towards the center of the turn; the lateral component of the NAF_{dorsal} corresponds to the centripetal force (CF). (B) A crabbed turn, in which a bat yaws into the turn. The yawing of the body will reorient the forward component of the net aerodynamic force ($NAF_{forward}$) produced during downstroke towards the center of the turn; the lateral component of the $NAF_{forward}$ corresponds to the centripetal force.

Brim-DeForest, 2008) and birds (Warrick and Dial, 1998; Hedrick and Biewener, 2007). However, crabbed turns are also phylogenetically widespread having been described in some dipterans (see Dudley, 2002), dragonflies (Alexander, 1986), gliding frogs (McCay, 2001) and gliding mammals (Bishop and Brim-DeForest, 2008).

For both banked or crabbed turns, body rotation results from an asymmetry in aerodynamic forces between left and right wings, an asymmetry in the inertial forces produced by the two wings or a combination of both. Aerodynamically generated force asymmetries can be expected as the result of differential changes in wing shape, such as changes in wing surface area, angle of attack, or camber or maybe due to differences between left and right wings in kinematic parameters, such as relative velocity (see Dudley, 2002). By contrast, inertially generated force asymmetries can be produced by differences in motion between left and right wings. Inertial forces can produce net changes in body orientation over a wingbeat cycle even when no external torques are applied due to conservation of angular momentum (Hedrick et al., 2007).

Moreover, little is known about the kinematics and aerodynamics of turning in bats, including whether they use primarily one, the other or both turning mechanisms. Whereas aerial maneuvers have been qualitatively described for two bat species (Norberg, 1976), and kinematics of the CoM have been analyzed for six other species performing 180 deg. turns (Rayner and Aldridge, 1985; Aldridge, 1987), no detailed analysis of body orientation and/or wing kinematics has yet been carried out for bats.

Photographs of bats performing flying maneuvers sometimes show the body rolled toward the direction of turning (Norberg, 1976). Based on this evidence and the widespread use of banked turns in organisms as morphologically and phylogenetically diverse as insects, amphibians, birds and mammals, we predicted that bats would also use banked turning and, therefore, maneuver by rolling their body to reorient the lift force vector.

MATERIALS AND METHODS

Experimental animals and flight corridor

The study animals were non-reproductive adult female lesser short-nosed fruit bats (*Cynopterus brachyotis* Muller 1838), loaned by the Lubee Bat Conservancy (Gainesville, FL, USA), housed at the Harvard University Concord Field Station (Bedford, MA, USA). Animals were provided with food and water *ad libitum* and kept in a large cage that allowed them to perform short flights. Four bats (body mass 32.8–41.7 g, N=4) were selected from among the captive population based in their consistent flight ability and cooperation during training sessions. Experimental subjects were trained to fly through an L-shaped flight corridor (7 m length×1 m width×2 m height) making a 90 deg. turn midway through each flight (Fig. 2). Bats were hand-released approximately 1.5 m above the ground on either side of the corridor, performed either a right or a left turn (depending on release site) and landed on the ceiling at the other end of the corridor.

Three-dimensional coordinate mapping

Each turn was recorded with three synchronized, high-speed digital video cameras: either three infrared-sensitive Redlake PCI 1000 cameras (320×280 pixel resolution; Redlake, San Diego, CA, USA) or two Redlake cameras and one Photron Fastcam-X 1280 PCI camera (1024×1024 pixel resolution; Photron USA, San Diego, CA, USA). Flights were recorded at 500 frames s^{-1} with shutter speeds of 1/1000th of a second. The cameras were placed on the floor of the flight corridor in such a way that at least one camera provided a cranioventral view and another provided a caudoventral view

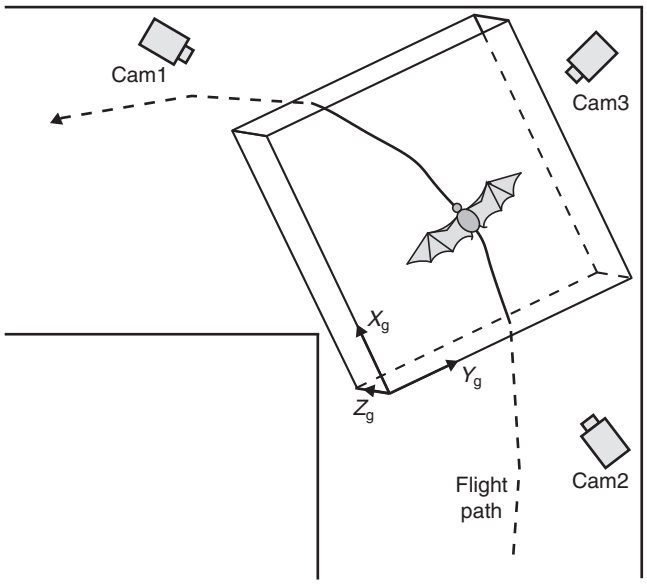

Fig. 2. Superior view of turning portion of the flight corridor, indicating the position of the calibrated space and the high-speed cameras. Three cameras were placed on the floor pointing upward to capture the ventral side of the bat body and wing. As the bat passed through the calibrated volume, the position of several anatomical markers were tracked in the global coordinate system $X_gY_gZ_g$. Figure not to scale.

(Fig. 2). Bats typically prefer low levels of visible light, therefore, illumination was provided by a series of infrared lights for the Redlake cameras and by a high-power red LED light for the Photron camera. The video files were calibrated by a modified direct linear transformation (DLT), a technique that computes 3-D coordinates from multiple known 2-D views, using a 25-point calibration frame (0.45×0.45×0.55 m) captured on video at the beginning of each series of flight (Hatze, 1988).

Lightweight spherical beads covered with reflective tape were attached to the pelvis on the skin overlying the pubic symphysis (*pvs* marker) and just lateral to the sternum (*Rch* and *Lch*, right and left chest markers, respectively). Chest markers were placed medial to the glenohumeral joint to ensure they remained in the field of view of the cameras as much as possible throughout the wingbeat cycle. Three additional anatomical landmarks on each wing: the wrist and the distal part of the distal phalanges of the 3rd and 5th digit (*wst*, *d3* and *d5*, respectively) (Fig. 3) were marked with small circular pieces of reflective tape.

A trade-off exists between maximizing the size of the cameras' field of view and maximizing spatial resolution of estimates of each marker's three-dimensional coordinates. In the present study, cameras were positioned to capture between two and four wingbeat cycles, depending on the flight speed of the bat in a particular trial. Sequences where all markers were visible for at least one complete wingbeat were digitized using custom-designed software (Hedrick, 2007). The three-dimensional position of each marker was reconstructed from the two-dimensional video files using the DLT coefficients derived from the calibration frame. Because of the great range of motion of the wing during flight, in some cases, markers were not visible in at least two cameras and the spatial position of the marker could not be resolved, resulting in gaps in the data. This was the case for the *wst* and *d5* markers at the beginning and at the end of the downstroke, in particular. Gaps, however, were relatively short and the curves were interpolated and filtered with the 'Generalized Cross Validatory Spline' (GCVSPL) software (Woltring, 1986). The spline smoothing coefficients were adjusted to produce a filter cut-off frequency of approximately 45 Hz, nearly five times greater than the wingbeat frequency. The quintic spline method also allows the direct calculation of higher-order derivatives and, therefore, provides greater accuracy in calculating velocities and accelerations (Walker, 1998). First and second derivatives of positional data were calculated from the spline coefficients, assuming no error and, hence, without further filtering.

To test the accuracy of our experimental setup, a spherical marker bead was thrown in a parabolic path through the calibrated space in front of the camera. Our calculation of its downward acceleration based on kinematic reconstruction was within 0.5% of 9.81 ms^{-1}. We also moved a rigid card with attached reflective markers at known separation distances similar to the intermarker distances on the wings of the bats as described above. Measurement error based on kinematic reconstruction was no more than 3% from the actual distances, with mean absolute errors ranging from 0.3 mm to 1.2 mm.

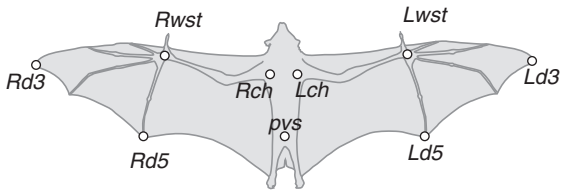

Fig. 3. Schematic representation of marker positions on the ventral side of a bat. Prefixes *R* and *L* refer to right and left, and *pvs*, *ch*, *wst*, *d3* and *d5* to pelvis, chest, wrist, end of the third digit and end of the fifth digit, respectively.

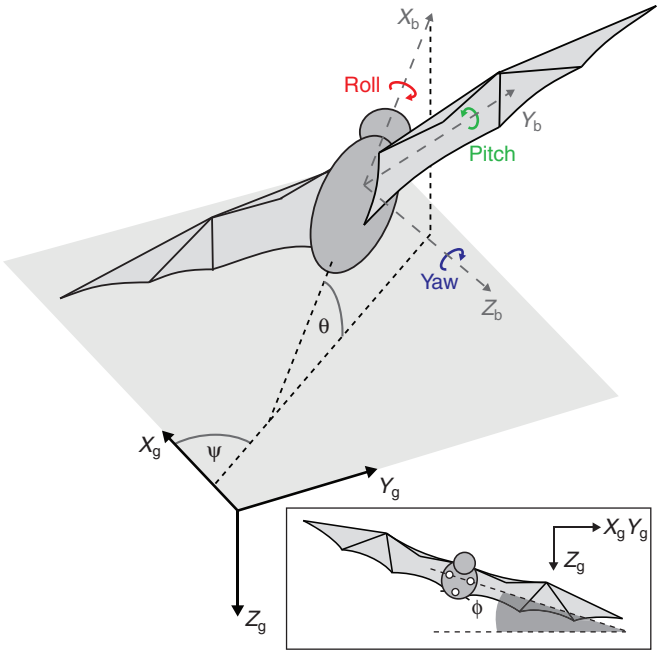

Fig. 4. Orientation and body angles used in the present study. The heading angle (ψ) was defined as the angle between the projection of the longitudinal axis of the body on the horizontal plane (X_g–Y_g) and the X_g axis; the elevation angle (θ) was defined as the angle between the longitudinal axis of the body and the horizontal plane (X_g–Y_g); and the bank angle (ϕ) was defined as the angle between the line connecting both chest markers and the horizontal plane (X_g–Y_g) (see inset). Body angles were defined as the deviation around the body-fixed axes in a body coordinate system. Arrows define the positive rotation direction of the body angles. Rotations about the body-centered $X_bY_bZ_b$ axes were designated roll, pitch and yaw, respectively. $X_bY_bZ_b$, dynamic, body-based coordinate system, centered on the hip.

Frames of reference, coordinate systems and body orientation angles

We employed two frames of reference to describe the positions of kinematic markers during turning (Fig. 4). First, an earth-fixed, global coordinate system $X_gY_gZ_g$ was defined, with X_g and Y_g describing the horizontal plane and with $+Z_g$ pointing in the direction of gravity. Second, we used a dynamic, body-based coordinate system $X_bY_bZ_b$, centered on the pelvis marker, where $+X_b$ points cranially along the body axis, $+Y_b$ points laterally toward the right wing, and $+Z_b$ points downward and lies in the plane of symmetry of the body. This frame of reference was defined by three coplanar body landmarks (*pvs*, *Rch* and *Lch*), and changed relative to the global coordinates as a bat moved through space. The body coordinate system was calculated from the global coordinate system using a series of Euler rotations for each time step. In an Euler angle system, three successive rotations about non-orthogonal axes define a unique attitude or general orientation of a rotated object with respect to a reference coordinate system. The first two Euler rotation angles described the heading (ψ) and elevation (θ) of the body with respect to the global coordinate system (Fig. 4). However, because of these rotations, the last rotation angle does not accurately

represent the bank orientation of the body with respect to the global coordinate system. Therefore, bank angle (ϕ) was calculated as the angle between the line connecting the two chest markers and the horizontal (X_g–Y_g) plane (Fig. 4, inset).

Body angles: yaw, pitch and roll

Rotations about the body-centered X_b, Y_b and Z_b axes were designated roll, pitch and yaw, respectively (Fig. 4), following aerodynamic conventions (Phillips, 2004). Body angular velocities were calculated by applying a classical transformation from the angular velocities of the Euler angles, commonly used in rigid body dynamics (Phillips, 2004). Because bats were recorded mid-turn, they already had an initial 'pitch' and 'roll' angles relative to the global coordinate system. These angles were added to the angular velocity cumulative sum and represent the angular body position with respect to the beginning of the recorded portion of the turn. Yaw initial orientation was arbitrary but because it has no systematic effect on flight control, all trials started with 0 deg. yaw angle [following Card and Dickinson (Card and Dickinson, 2008)]. Body angular accelerations were calculated as the first derivative of the body angular velocities over time.

Determination of CoM

Although the wings of the bat comprise a relatively small fraction of the overall mass of the bat (Thollesson and Norberg, 1991), the motions and accelerations associated with wing flapping may produce substantial inertial effects. As a result of these morphing motions, the CoM of the bat will not correspond to a fixed anatomical location on the bat during flight. To account for the wing displacements in the determination of the location of the CoM, we constructed a mass model representation of the bat.

The mass model is a time varying, discrete mass approximation of the bat mass distribution based on the location of the markers. To develop the discrete mass system representing the bat, we partitioned total body mass into individual components or regions. The wing membrane, wing bones and trunk were treated as separate masses, which were combined to form the total mass model.

To model the mass distribution of the membrane, we constructed a triangulation of the wing geometry at each time step. The large-scale, base triangulation was developed using the location of the marker positions at any given time, and a subsequent subdivision of these triangles was performed to give a mesh of fine-scale triangular elements (Fig. 5). Each triangle element (T_i) on the membrane was assigned a constant thickness (1×10^{-4} m) and density (1×10^{3} kg m^{-3}), based on measured characteristics of bat wing membrane skin (Swartz et al., 1996). A resulting discrete point mass (m_i) for each triangular membrane element was computed based on the volume of that triangular membrane and assigned a position at the centroid of the triangle element. To model the distribution of mass among and within each of the wing bones, we constructed a curve between the markers at the endpoints of the bones. The curve for each bone in the wing was defined from the location of the markers, and the mass of the fourth digit, that we did not track, was divided equally between the third and fifth digit. Given the tapered shape of bat bones (Swartz, 1997), the cross-sectional radius of each bone element of the model was defined by a quadratic function with respect to the length of the bone. We assigned a constant density to the bones (2×10^{3} kg m^{-3}). Using the distribution of bone radii distribution and the location of the bone elements in space, the line was subdivided into smaller line-elements from which discrete mass points were defined. The mass of the wings was scaled such that the constructed distribution represents 16% of the total body mass, according to measurements of bats of similar size (Thollesson and Norberg, 1991). The mass and moment of inertia of the wing with respect to the shoulder were compared with measured values (Thollesson and Norberg, 1991) to ensure that the model represents the physical reality. Finally, the bat's body was defined as a three-dimesional ellipsoid divided into discrete mass points.

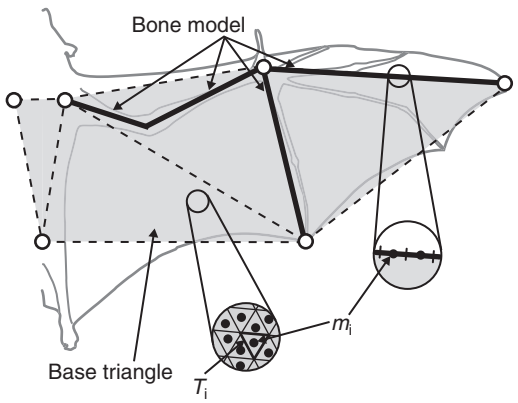

Fig. 5. Schematic of the mass distribution model used to calculate the center of mass (CoM) of the bat. The thick, solid lines represent the modeled masses of the bone. The shaded triangle patches represent the base triangles of the skin mass model, and insets show detailed subdivisions of bone and skin masses (m_i) and individual triangular elements (T_i) of the model.

The discrete mass representation of the membranes, bones and body were combined with detailed kinematic records of motion of each landmark to determine the CoM of each of the mass elements, m_i, using the equation:

$$\vec{r}_{CoM} = \frac{\sum \vec{r}_i\, m_i}{m_T}, \quad (1)$$

where $\vec{r}_{CoM}$ represents the position vector of the CoM, $\vec{r}_i$ represents the position vector of the i-th discrete point mass and m_T represents the total mass of the bat.

Calculation of kinematic parameters

Velocity, acceleration, changes in heading and curvature

Net body velocity ($\mathbf{V}_b$) and acceleration ($\mathbf{A}_b$) vectors were calculated as the first and second derivatives of the position vector of the CoM in the global coordinate system. The global trajectory of the bat (i.e. the flight direction) in the horizontal plane was defined as the bearing angle (φ) and was calculated as the angle between the horizontal component of the net body velocity vector ($\mathbf{V}_{b,xy}$) and the X_g axis (Fig. 6). Changes in heading can be described as a rate of turning known as curvature (κ). Curvature is defined as the inverse of the radius of the curved path and is calculated by the equation:

$$\kappa = \frac{\left|\mathbf{V}_{b,xy} \times \mathbf{A}_{b,xy}\right|}{\left|\mathbf{A}_{b,xy}\right|^3}, \quad (2)$$

where $\mathbf{V}_{b,xy}$ and $\mathbf{A}_{b,xy}$ are the velocity and acceleration of the body in the horizontal plane X_g–Y_g, respectively.

Angle of attack and wing surface area

Differences in the angle of attack of the two wings during a wingbeat cycle could have aerodynamic influence that results in turning. Angle

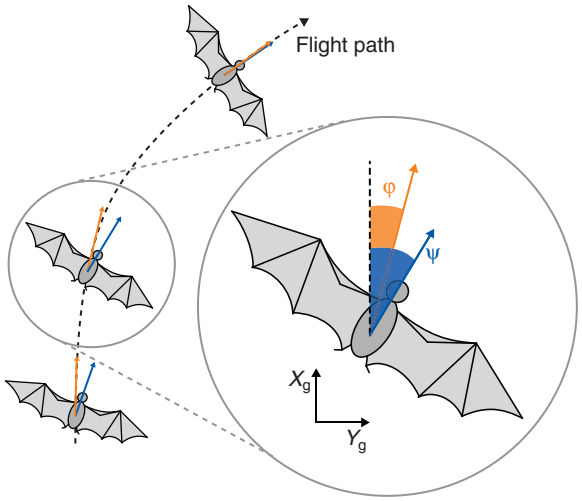

Fig. 6. Dorsal view of a flying bat showing the relationship between bearing angle (φ) and heading angle (ψ) in the global coordinate system for a bat at three time points during the turn. Bearing angle is calculated from the horizontal component of the body velocity vector ($V_{b,xy}$, orange arrows) obtained as the derivative of the position vector of the center of mass (CoM). The heading angle (ψ) was defined as the angle between the projection of the longitudinal axis of the body on the horizontal plane (X_g–Y_g) and the X_g axis.

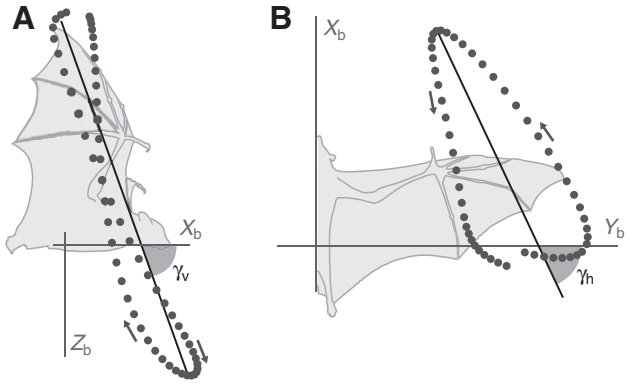

Fig. 7. Lateral (A) and dorsal view (B) of a flapping bat, indicating vertical (γ_v) and horizontal (γ_h) stroke plane angle in the body coordinate system. Dotted line corresponds to an actual trace of the right wingtip (*d3* marker) throughout a representative stroke cycle.

of attack was calculated for each wing as the angle between the relative incident air velocity of the wrist marker (*wst*) and the plane of the hand wing, defined by the markers on the wrist (*wst*), fifth digit (*d5*) and the wingtip (*d3*). The exact calculation of the angle of attack requires the estimation of the induced velocity on the wing (i.e. wake and wing-bound vortex velocities) (Aldridge, 1986b); however, we ignored induced velocity because our analyses focus on comparisons between left and right wings, and induced velocities are similar for the two wings.

The difference in the surface area between left and right wing was estimated in two ways: (1) by calculating the wrist angle, a measure of the flexion/extension of the wing as a proxy and (2) by the lateral distance of the wingtip marker (*d3*) with respect to the midline of the body in a body coordinate system. Wrist angle was defined as the interior angle of the triangle formed by the chest (*ch*), wrist (*wst*) and wingtip (*d3*) markers for each wing. Thus, when wrist angle and the lateral distance of the wingtip marker are large, wing surface area is also expected to be large.

Downstroke, upstroke and stroke plane angle

Downstroke and upstroke phases of the wingbeat were defined by positive and negative velocities of the wrist in the Z_b direction, respectively. The vertical (γ_v) and horizontal (γ_h) stroke plane angles were defined as the major axis of the projection of the wingtip with respect to the body on the X_b–Z_b and X_b–Y_b planes, respectively (Fig. 7). These major axes were estimated by fitting a least-square line for each wingbeat.

Lateral projection of the wings

Changes in body rotations could be potentially explained by differences in profile drag produced between the two wings. A possible mechanism to modulate drag is to alter the wing area exposed to the airflow. Lateral projection of the wing can be used as a proxy for wing area exposed, where wings that are more extended should present larger wing areas. We estimated the lateral projection as the distance of the wingtip marker to the midline of the body in the global coordinate system.

Wingbeat consolidation and statistical analyses

To avoid the problem of autocorrelation and pseudoreplication among wingbeats, kinematic parameters were calculated from one representative wingbeat per trial. We defined the representative wingbeat as the one with a heading angle the closest to 45 deg. from the initial orientation of the flight. This wingbeat represented a mid-turn wingbeat and usually represented the maximum angular velocities of both heading and body angles. In some cases, angular velocities peaked ±1 wingbeat from the wingbeat defined by the heading angle criterion. In such a case, the angular velocity criterion was used. For most of the analyses, a sample size of 32 trials was used and values are reported as means ± s.e.m., unless specifically indicated. Statistical analyses were conducted using JMP 6 (SAS Institute, Cary, NC, USA) and MATLAB R2006a (The Mathworks, Natick, MA, USA). Regression analyses were performed with general linear models (GLM) to control for differences among individuals.

RESULTS

General description of the turn

When turning, bats flew consistently at low forward speeds of 2.0±0.1 ms^{-1} (N=53) and maintained relatively constant speed in the X_b direction throughout the calibrated volume, although in four trials, flight speed decreased at the end of the sequence. In a typical turn, bats gained altitude during the first half of the turn (0.12±0.04 m, N=53) and then maintained their height after turning, thereby increasing their net altitude during the turn.

Changes in bearing occurred almost entirely during the downstroke (Fig. 8), with a mean change of 16.0±0.8 deg. $wingbeat^{-1}$. Depending on the flight speed, we captured between two and four wingbeats within the calibrated space. Extrapolating the mean change in heading during a wingbeat cycle to the whole turn, *C. brachyotis* would complete a 90 deg. turn in approximately 6–7 wingbeats. This is likely to be an overestimation as the change in heading tends to peak towards the middle of the turn. From a preliminary study of *C. brachyotis* performing the same task, a 90 deg. turn was completed in approximately 6–9 wingbeats (J.I.-D., unpublished). Bats reached maximum changes in bearing of 416.9±26.4 deg. s^{-1} near mid-downstroke, producing turns with a

minimum turning radius of 0.290±0.031 m (curvature of 5.53±0.62 m^{-1}), approximately 0.8 wingspans. Mean curvature during downstroke was 3.36±0.33 m^{-1}.

Changes in body orientation

Bats consistently changed their body orientation throughout the wingbeat cycle in a sinusoidal fashion with a frequency equal to the wingbeat frequency (Fig. 8). Bats rolled into a bank at the beginning of the turn. Mean bank angle over a wing stroke was 25.8±2.0 deg. with a maximum of 56.3 deg. Bank angle reached a maximum at mid-downstroke and a minimum at mid-upstroke with an absolute change of 10.6±1.1 deg. half-stroke^{-1}. Despite the apparent variation within a wingstroke, mean bank angle did not change among wingbeats within each trial (paired *t*-test, t_{31}=0.84, P>0.1) (Fig. 9A). Similarly, elevation angle showed changes within the wingbeat cycle, with a mean difference of 10.6±1.1 deg. per half-stroke, reaching a maximum at mid-downstroke and a minimum at mid-upstroke but with no significant changes between wingbeats (paired *t*-test, t_{31}=–1.55, P>0.1) (Fig. 9A). Mean elevation angle was 25.7±2.5 deg. Heading angle, however, showed a significant between-wingbeat component (paired *t*-test, t_{31}=13.58, P<0.0001), as expected in a turn, as bats have to continuously change their body orientation to keep it aligned with their bearing (Fig. 9A). During upstroke, bats increased their heading angle by a mean of 20.8±1.9 deg., rotating towards the direction of the turn.

Angular velocity and angular acceleration profiles were very similar for all three angles (Fig. 9B,C). During upstroke, angular velocities increased reaching a peak around the upstroke-downstroke transition of 363.5±23.7, 217.2±20.5 and 104.3±23.3 deg. s^{-1} for heading, elevation and bank angles, respectively (Fig. 9B). Angular accelerations showed a clear pattern of positive acceleration for all three angles throughout upstroke and a very strong negative acceleration around the middle of the downstroke (Fig. 9C).

Changes in body angles

Pitch angle showed high within-wingbeat variation, reaching a minimum at mid-upstroke and a maximum at mid-downstroke, with a mean change of 12.1±0.9 deg. half-stroke^{-1} (Fig. 9D). Yaw angle increased constantly throughout the wingbeat (Fig. 9D) and showed a difference of 13.7±1.0 deg. between the end and the beginning of the wingbeat (paired *t*-test, t_{31}=12.4, P<0.0001) that resulted from positive yaw angular velocities throughout the wingbeat (Fig. 9E). By contrast, roll angle decreased over the wingbeat, decreasing during the upstroke and remaining constant during downstroke (Fig. 9D). Over a wingbeat cycle, roll angle decreased –4.3±1.1 deg. (paired *t*-test, t_{31}=–4.0, P<0.0001). Yaw angular velocity was positive throughout the wingbeat, in contrast to roll angular velocity, which was mostly negative (Fig. 9E).

Pattern of change in heading and flight direction

Heading and bearing angle varied in a similar fashion throughout the wingbeat cycle, with changes of similar magnitude but with a clear offset between them (Fig. 8A; Fig. 10A). Heading angular velocity peaked at the upstroke–downstroke transition, although bats changed bearing the most at the middle of the downstroke (Fig. 10B),

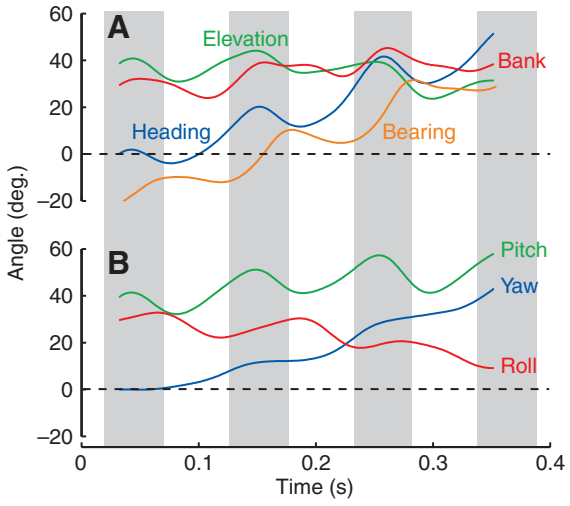

Fig. 8. Plot of the orientation angles (heading, bank and elevation; A) and body angles (yaw, pitch and roll; B) for a representative right turn. Bearing angle (orange line) was included to the orientation angles plot for comparison of body attitude with the changes in flight direction. Shaded bars correspond to downstroke periods.

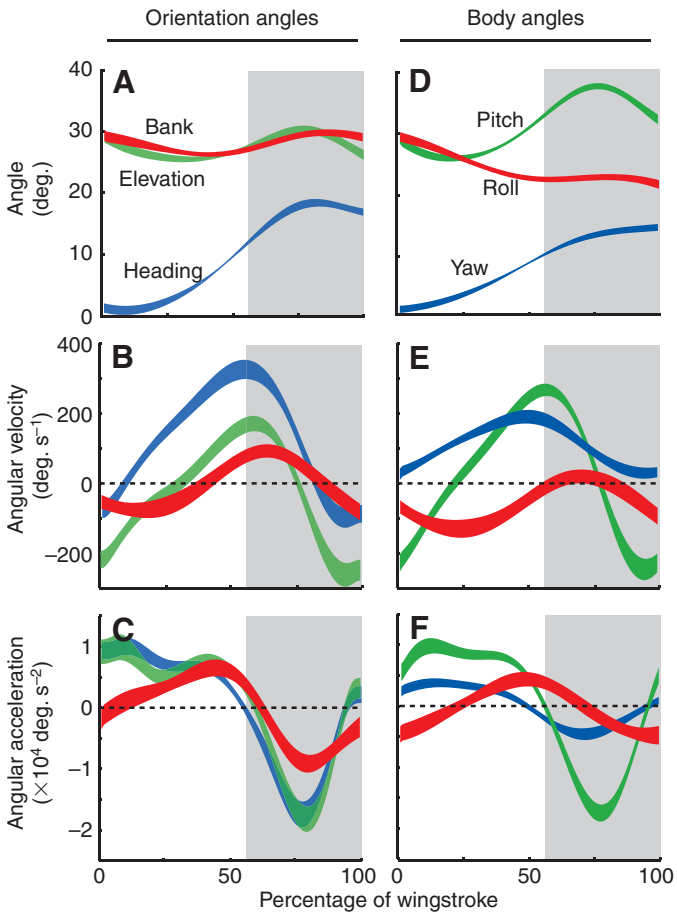

Fig. 9. Angle, angular velocities and angular accelerations for the orientations angles (heading, elevation and bank) (A–C) and the body angles (yaw, pitch and roll) (D–F). The width of the traces represents the means ± s.e.m. Shaded bars correspond to downstroke periods. Because bats performed both right and left turns, all turns were standardized to a right turn, and both heading and yaw angles started at zero degrees. Body angles were obtained as the cumulative sum of the body angular velocities obtained from the angular velocities of the Euler angles. For pitch and roll angles, the cumulative sum was added to the initial elevation and bank angle, respectively, for each trial.

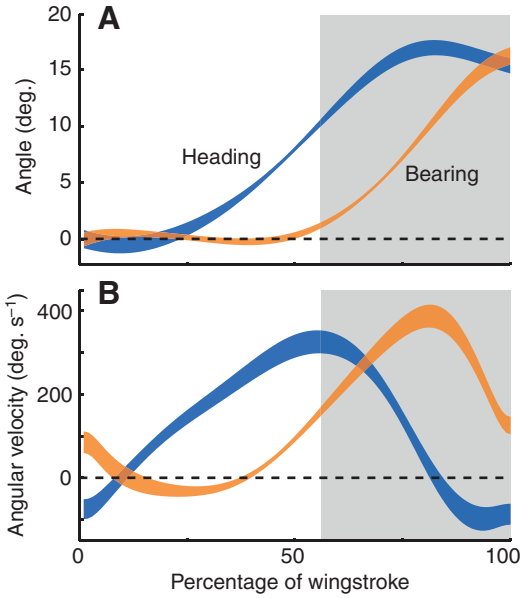

Fig. 10. Angle and angular velocity for heading (blue trace) and bearing (orange trace) throughout a stroke cycle measured in a global coordinate system. Shaded bars correspond to downstroke periods. The width of the traces represents the means ± s.e.m.

indicating that changes in heading preceded changes in flight path during the turn. The difference between heading and bearing angle peaked at the upstroke–downstroke transition and reached a minimum at the end of the downstroke (Fig. 10A).

Wingbeat kinematic parameters

Bats flew using wingbeat frequencies of 9.2±0.1 Hz, with upstrokes comprising 56±2% of the stroke cycle. Wingtip speed with respect to the body showed a sinusoidal variation with a frequency of nearly half of wingbeat frequency (Fig. 11A). Wingtip speed reached a minimum of 4 m s^{-1} at mid-upstroke and a maximum of about 8 m s^{-1} near the end of upstroke and at mid-downstroke (Fig. 11A). Wrist velocity showed less variation during the stroke cycle with a mean speed near 3 m s^{-1} (Fig. 11B). Mean downstroke speed was 6.31±0.11 and 2.97±0.10 m s^{-1}, for the wingtip and wrist, respectively. During a half-stroke, angle of attack changed from approximately 50 deg. at the beginning of downstroke to approximately 20 deg. at the end of downstroke with a mean of 26.7±0.7 deg. Vertical stroke plane angle, γ_v, was 52.7±4.8 deg.

Wing kinematics in the body coordinate system were very similar for the inside and outside wings; however, small but statistically significant asymmetries were observed. Mean wingtip speed of the inside wing was 7% faster (a difference of 0.27±0.15 ms^{-1}; paired t-test, t_{31}=1.82, P=0.08), particularly during the upstroke (Fig. 11A). No significant differences in speed between the two wings were observed at the wrist (Fig. 11B). These differences are mostly due to higher wingtip lateral velocities of the inside wing during the beginning and the end of the upstroke (see Fig. S1F in supplementary material).

The angle of attack of the inside wing during downstroke was 9% larger (a difference of 2.7±0.9 deg., paired t-test, t_{31}=3.15, P<0.01) than the outside wing (Fig. 11C). Also, the wrist angle, a measure of the extension of the hand, and likely of the surface area of the wing, was larger in the inside wing by 3.3±0.7 deg. (paired t-test, t_{31}=4.18, P<0.001) (Fig. 11D). Even though elbow angle was not measured, we believe that this angle reflects overall wing extension as we also found no major differences in the distance of the wingtip to the midline of the body throughout the wingbeat (see Fig. S1A,E,I in supplementary material). The largest kinematic difference was found in the horizontal stroke plane angle γ_h. The asymmetry in γ_h during turning was 10.8±2.8 deg. (paired t-test, t_{31}=3.86, P<0.001), indicating that the outside wing moved more parallel to the long axis of the body than the inside wing, which had an overall direction more oriented towards the midline.

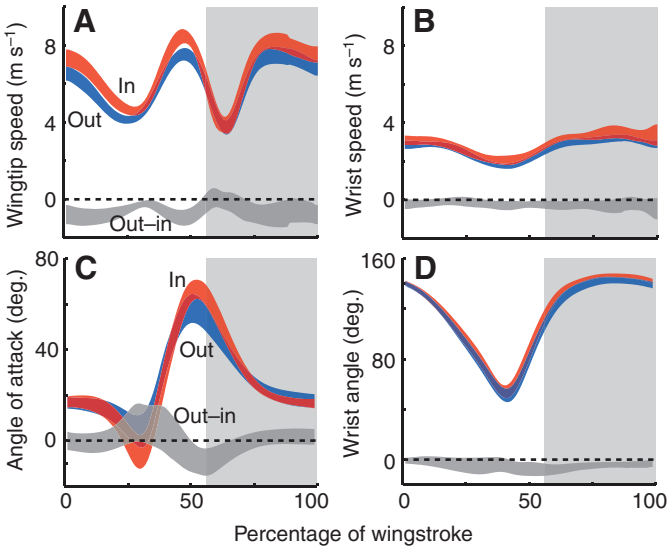

Fig. 11. Speed of wingtip marker (A), wrist marker (B) in the body coordinate system, angle of attack (C) and wrist angle (D) over a standardized wingstroke. Red, blue and grey traces represent the inside and the outside wing and the difference between them, respectively. The width of the traces corresponds to the 95% CI (confidence interval). Shaded bars correspond to downstroke periods.

Kinematic correlations with changes of direction

In a banked maneuver, the centripetal force that produces the turn depends on the bank angle: the greater the bank angle, the greater the centripetal force and the tighter the turn. In such a case, the rate of change in direction angle is expected to be proportional to the bank angle (McCay, 2001). However, in a crabbed maneuver, the change in direction should be related to the rate of change in heading rather than heading orientation (Warrick et al., 1998; Hedrick and Biewener, 2007). Both heading angular velocity and mean bank

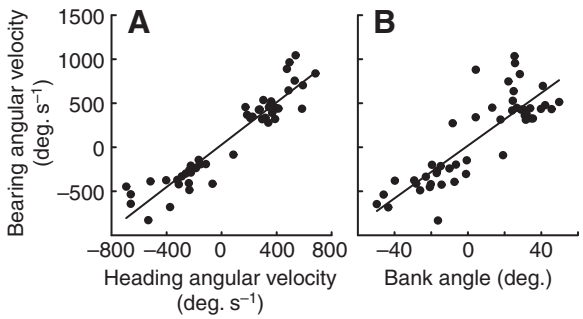

Fig. 12. Relationship between heading angular velocity (A) and bank angle (B) with the bearing angular velocity.

angle during the downstroke are significantly correlated with the peak rate of change in direction (GLM, r^2_{adj}=0.88, $F_{4,44}$=92.7, P<0.0001 and GLM, r^2_{adj}=0.72, $F_{4,44}$=32.48, P<0.0001, respectively) (Fig. 12). In a multiple regression model, controlling for individual effects, only heading angular velocity was significant (GLM, r^2_{adj}=0.89 for the whole model; heading angular velocity effect, β=0.82, $F_{1,43}$=63.5, P<0.0001; bank angle effect, β=0.13, $F_{1,43}$=1.6, P>0.2). The partial correlation between heading rate and bearing rate when controlling for bank angle was $r_{heading|bank}$=0.80 (two-tailed t-test, P<0.0001) whereas the partial correlation between bank angle and bearing rate when controlling for heading angular velocity was $r_{bank|heading}$=0.14 (two tailed t-test, P>0.05).

Based on the instantaneous acceleration of the CoM estimated from the mass model (see Materials and methods), it is possible to calculate the total instantaneous centripetal acceleration ($\mathbf{A}_{c,total}$) necessary to produce a turn with a radius 1/κ using:

$$\mathbf{A}_{c,total} = (\mathbf{V}_{b,xy})^2\kappa, \quad (3)$$

where $\mathbf{V}_{b,xy}$ is the forward speed of the estimated CoM in the horizontal plane of the lab X_g–Y_g, and κ is the curvature of the turn. Given the symmetry in the wing kinematics in the body coordinate system, we can estimate the centripetal component produced by the banked orientation of the body by assuming that the net aerodynamic force is oriented perpendicular to the bank angle (Fig. 13A). Thus, the bank component of the centripetal acceleration was estimated as:

$$\mathbf{A}_{c,bank} = (\mathbf{A}_{CoM,z} + \boldsymbol{g}) \tan\phi \cos(\psi - \varphi), \quad (4)$$

where $A_{CoM,z}$ corresponds to the vertical acceleration calculated from the position of the CoM, and $\boldsymbol{g}$ corresponds to the acceleration of gravity (Fig. 13A,B). On average, $\mathbf{A}_{c,bank}/\mathbf{A}_{c,total}$, the estimated centripetal acceleration produced by the degree of bank relative to the centripetal acceleration necessary to produce the observed change in flight direction, accounted for only 74.0±4.9% of the total acceleration required (Fig. 13C). In three trials, the bank contribution was as small as 10% of the necessary centripetal acceleration, and in five trials, bank angle accounted for more than 90% of the acceleration needed to produce the turn.

Lateral projection of the wings

The lateral projection of the wing was maximal during downstroke for both wings (Fig. 14). The wingtip of the inside wing started to move laterally during the second half of the downstroke, while the outside wing was extended during downstroke as a consequence of the bank of the body during the turn. During the second half of the upstroke, the inside wing projected further than the outside wing, which could have created greater drag on the inside wing due to a larger wing area (Fig. 14). Accordingly, the difference of the lateral projection of the wingtip between wings significantly predicts the observed changes in global yaw angular velocity at the upstroke-downstroke transition (GLM, whole model, r^2_{adj}=0.56; distance effect, $F_{1,24}$=12.0, P=0.002).

DISCUSSION

Bats carried out low speed 90 deg. turns by using a combination of crabbed and banked mechanisms to redirect their net aerodynamic force and, thus, produce centripetal force towards the direction of the turn. We found that turns can be divided into two temporally different components associated with the portions of the wingstroke cycle. In the first part of the turn, during upstroke, bats rotated their bodies horizontally into the turn without significant changes in flight direction. As a result, at the onset of downstroke, the body was

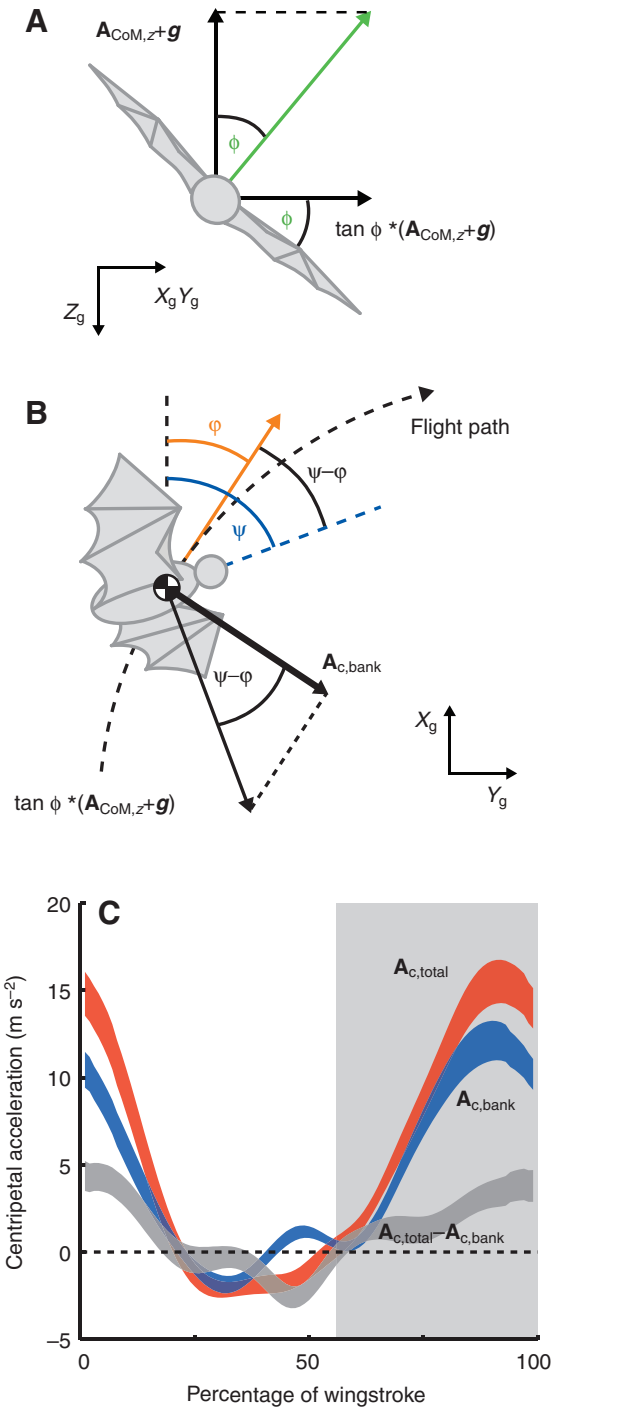

Fig. 13. Effect of bank angle and heading on the estimation of the expected centripetal acceleration due to the banked orientation of the body. (A) Posterior view of a bat performing a right turn. The net aerodynamic force (green vector) was estimated based on the bank angle (ϕ), the total vertical acceleration produced by the bat ($\mathbf{A}_{CoM,z}$), and assuming that the net aerodynamic force is produced perpendicular to the bank angle. (B) Superior view of a bat performing a right turn. Because the heading orientation of the body (blue line) does not necessarily match the direction of flight (orange vector), the centripetal acceleration due to the bank ($\mathbf{A}_{c,bank}$) must be corrected by the difference between heading and bearing angle (ψ–φ). (C) Observed ($\mathbf{A}_{c,total}$, red trace) and the estimated centripetal acceleration from bank ($\mathbf{A}_{c,bank}$, blue trace) throughout a standardized wingstroke. Gray trace corresponds to the difference $\mathbf{A}_{c,total}$–$\mathbf{A}_{c,bank}$. The width of the traces represents the means ± 95% CI (confidence interval) (N=32) and the shaded bar corresponds to the downstroke period.

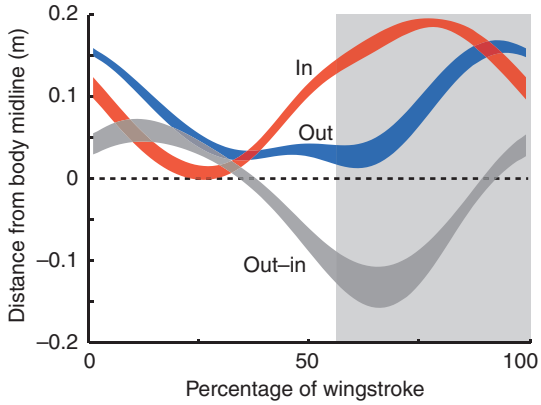

Fig. 14. Distance of the wingtip to the midline of the body in the horizontal plane X_g–Y_g, and red, blue and gray traces correspond to the inside (in) and the outside (out) wing and the difference between them (out–in), respectively. The width of the traces corresponds to the 95% CI (confidence interval). Shaded bar corresponds to the downstroke period.

already oriented toward the direction of the turn so that forward component of the net aerodynamic force was also oriented towards the center of the turn. In the second part of the turn, which occurred during downstroke, bats changed their flight direction. However, the centripetal force necessary to change the heading of the CoM was produced by a combination of the forward and the dorsal component of the net aerodynamic force. The dorsal component, which is parallel to the mid-sagittal plane of the bat's body, arose from the banked attitude of the body through which the vertical component of the net aerodynamic force was reoriented toward the center of the turn. The forward component was modulated by the heading rotation of the body that occurred during the first part of the turn. The analyses presented in the current study do not fully support our prediction that bats use a banked turning mechanism, similar to those described for other flying organisms. However, our results indicate that turning in bats is aerodynamically and kinematically complex, and highlights the importance of the upstroke phase, usually ignored in studies of animal flight.

Kinematic mechanisms affecting change in heading

Discussions of turning in flying vertebrates have focused almost exclusively on the reorientation of the lift vector by rolling the body into a bank as the mechanism for the generation of the centripetal force (Norberg, 1990; Dudley, 2002). However, the results of the present study demonstrate that for *C. brachyotis*, change in heading was the best predictor of the change in flight direction. By rotating their bodies horizontally during upstroke, bats reoriented their major body axis in the direction of the turn. As a consequence, when aerodynamic force was produced during downstroke, the thrust vector was already oriented in the direction of the turn (Fig. 1). Although the bank angle did not significantly explain changes in flight direction when changes in heading are considered, the banked orientation of bats observed during downstroke will probably produce centripetal forces nonetheless. Our estimations of the centripetal accelerations produced by the banked orientation suggested that bats produced approximately 70% of the necessary force required to generate the observed turn. This figure, however, is likely to be an overestimate. We assumed that the net aerodynamic force was perpendicular to the horizontal plane of the bat but the larger angle of attack of the inside wing compared with the outside wing during the downstroke would probably displace the net aerodynamic force vertically, reducing the role of banking with respect to changes in heading. Thus, we hypothesize that there will be a synergistic effect of the changes in heading during upstroke and the banked attitude of the body that will increase the amount of centripetal force produced by either a banked or crabbed turning alone.

Offset between changes in heading and changes in flight trajectory

It has been suggested that when a flying organisms does not bank, changes in bearing in crabbed turns are functionally linked to changes in heading angles such that flight trajectory would change only when yaw angle changes (Warrick et al., 1998). This assumes, however, that the yaw moment is produced by differential generation of thrust between the left and right wings during downstroke. This is clearly not the case for *C. brachyotis* where changes in heading preceded changes in bearing (Fig. 10A). The offset between body rotations and changes in flight trajectory implies that, at the beginning of the downstroke, a bat's cranio-caudal axis is already partially oriented toward the turn. As a consequence of this body orientation, the forward component of the net aerodynamic force (NAF) will also have a centripetal component that adds to the centripetal component produced by the bank *per se*. Therefore, we hypothesize that the temporal offset between body rotations and changes in flight direction increases the centripetal force generated in comparison with that generated by a banked turn alone. Such an offset could be particularly important for turns during slow flight, in which air flow over the wings is relatively slower and, thus, contributes less to lift generation than in high-speed flight.

Changes in body orientation prior to changes in heading may also improve the ability of a flying animal to orient the head to the direction of travel, therefore, improving spatial orientation. Insectivorous bats clearly orient the head toward the insect when pursuing maneuverable or erratic prey, and change their flight direction accordingly to keep the body aligned with the head direction (Ghose and Moss, 2006). In this case, rotating the body before changing heading would facilitate alignment of the head and body to increase prey location and obstacle avoidance success (Ghose and Moss, 2003; Ghose et al., 2006). The fact that we observe alignment of the body with flight direction on a non-echolocating, fruit-eating bat suggests that this phenomenon would be important not only when emitting echolocation calls and listening for returning echoes and when capturing prey but also simply to maneuver successfully in three-dimensionally complex environments.

Effect of body-based rotation angles (yaw, pitch and roll) on turning

Because bats adopt a banked attitude during the turn, changes in heading angle require changes in both pitch and yaw. Our results indicated that pitch is particularly relevant, showing significant variation throughout the wingbeat cycle and higher angular accelerations than yaw. This suggests that a significant portion of the change in heading derives from changes in pitch. This, in turn, informs our understanding of the forces necessary to rotate the body. A body's rotation about its CoM depends on its mass moments of inertia and on the moments about each axis. In organisms with elongated bodies, it is assumed that the moment of inertia around the roll axis is smaller than the moment of inertia around the yaw and pitch axes (e.g. Dudley, 2002), suggesting a faster rotational response to roll than to yaw or pitch. However, rolling moments in these bats seem to be mostly compensatory with changes in the

opposite direction to the turn, resulting in an approximately constant bank angle (Fig. 9A,D).

There are advantages of employing modulation of pitch to perform turns. Assuming that there is a trade-off between bilateral wing motion asymmetry and the efficiency of lift and thrust that are produced, pitch can be adjusted by bilaterally symmetrical changes in wingbeat kinematics that shift the net aerodynamic force vector either anterior or posterior to the CoM whereas changes in yaw and roll require bilateral asymmetries (Dudley, 2002). Furthermore, pitch modulation may also require less force than is required to produce rotational changes in yaw. The contribution of the wings to the total mass and to the moment of inertia can be considerable in bats (Kirkpatrick, 1990; Watts et al., 2001). For example, in a study of eight bat species, the mass of one wing accounted for approximately 8% of the total body mass and contributed to approximately 93% of the roll inertia (Thollesson and Norberg, 1991). In this example, yaw inertia is expected to be larger than pitch moment of inertia assuming that the pitch rotational axis passes through the wings. It is interesting to note that flapping fliers, even in straight, level flight at constant velocity show up and down pitching moments during upstroke and downstroke, respectively. However, comparison of the effect of these 'natural' pitching moments with those observed on turning flight is not straightforward due to the banked orientation of the bat. Pitching moments are the result of both inertial and aerodynamic effects. Although changes in pitch due to inertial forces are not expected to change when bats are in a bank turn compared with when they are in straight flight, we do expect changes in how aerodynamic forces would affect pitch due to the differences in orientation of the gravitational force with respect to the net aerodynamic force.

Mechanisms of heading rotation

Changes in heading are essential to the completion of the turn. However, we observed that heading rotation in the direction of the turn occurs mostly during the upstroke. This portion of the wingbeat cycle, at least for slow flight, has been believed to be inactive aerodynamically (Norberg, 1990; Spedding et al., 2003). How, then, are bats able to change their heading orientation during the upstroke? One mechanism for producing changes in heading is to generate more thrust with the outside wing than with the inside wing, producing a torque in the direction of the turn. This could potentially be accomplished by a backward flick with the tip of the wing, which has been reported in some bats at the beginning of the upstroke when flying at low speeds (Aldridge, 1986b; Norberg and Winter, 2006). Such a backward flick is observed in *C. brachyotis* at the wingtip (Fig. 15A) but not at the wrist (Fig. 15B) and it is unlikely to produce a global yaw moment because the backward velocities of the outside and the inside wing do not differ significantly during the upstroke (Fig. 15A).

Differences in profile drag between the inside and outside wing could also potentially produce changes in heading by modulating the drag generated by each wing. The lateral projection of the wings suggest that differential drag between the inside and outside wing may act during upstroke, as the inside wing was more laterally projected than the outside wing during late upstroke. Differences in the lateral projection of the wings and the heading velocity reached at the upstroke–downstroke transition were significantly correlated, suggesting that differential drag due to differences in left *vs* right wing area could explain the changes in the global yaw observed for *C. brachyotis*. The precise physical mechanism underlying this correlational result must be considered unknown at present because estimates of torque about the vertical global axis require

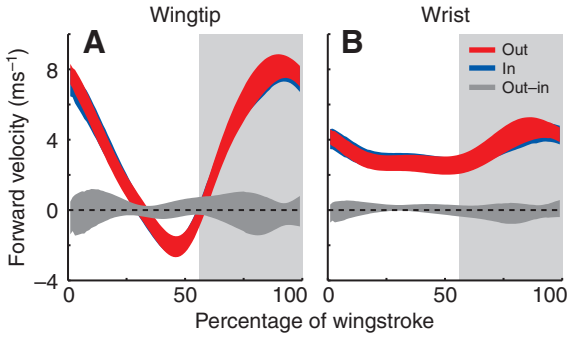

Fig. 15. Forward velocity profiles for the wingtip (A) and wrist markers (B) in a global coordinate system that has been rotated in the Z_g axis to align the *X*-axis component to the bearing velocity vector and, thus, the forward velocity represents the marker velocity in the direction of flight. This rotation maintains the elevation and bank orientation of the body. The width of the traces represents the means ± 95% CI (confidence interval). Shaded bars correspond to downstroke periods. In, inside of the wing; out, outside of the wing; out–in, difference between outside and inside wing.

consideration of aerodynamic angles of attack and, therefore, of the direction of the aerodynamic force produced by the wings. To verify this, calculations of the profile drag generated by each wing will be necessary, which requires estimates of coefficient of drag during upstroke. Due to the three-dimensional complexity of the wing shape during upstroke, and the lack of empirical estimates of the drag coefficients of compliant airfoils, results from steady-state calculations will probably be too unreliable to shed much light on this question.

An alternative means by which to produce changes in heading is the use of asymmetric movements of the wings during upstroke. Left–right asymmetry could generate inertial torques that differ between the inside and outside wing. Such a mechanism is an effective way to produce what is called a zero-angular-momentum rotation, a maneuver used by self-righting cats (e.g. Arabyan and Tsai, 1998) and gymnasts (Yeadon, 1997). In a zero-angular-momentum rotation, body segments are rotated with respect to each other during flight, hence, the whole body will rotate as a consequence to conserve angular momentum. By this mechanism, changes in heading would arise from differences in the movement of the left and right wings in the horizontal X_g–Y_g plane. It is difficult to predict the effect of wing and body inertia on the body rotation without modeling the time-varying contribution of a morphing wing and rotating body during the turn but considering the wing masses of bats are approximately 16% of total body mass (Thollesson and Norberg, 1991), it could be expected that inertial reorientation of the body may be important. Inertial contributions to body rotations during turning have been estimated for birds where asymmetries in the amplitude of the wingbeat were capable of transient changes in roll of only 6 deg., with a net change of 1.6 deg. per wingbeat (Hedrick and Biewener, 2007). Bats are expected to have a smaller moment of inertia for roll than for yaw and pitch, hence, the magnitude of changes due to inertial reorientation in yaw are not likely to be great enough to account for the mean change of 20 deg. in yaw observed during upstroke. However, this issue cannot be resolved without modeling the inertial effect of the observed wing kinematics.

Bat turning compared with other flying organisms

Experiments on maneuvering in birds show that pigeons and cockatiels use banked turns (Warrick and Dial, 1998; Hedrick et al., 2002). In

pigeons, roll acceleration increases and decreases during a single wingbeat, and changes in acceleration are correlated with left–right asymmetry in downstroke wing velocity (Warrick and Dial, 1998). Cockatiels show a similar roll acceleration profile, with changes in roll orientation within each wingbeat correlated with wing motion asymmetries (Hedrick and Biewener, 2007). This within-wingbeat variation, however, is probably the result of inertial forces produced by wing kinematic asymmetries and, therefore, tends to cancel out over a complete stroke cycle (Hedrick and Biewener, 2007). In fact, changes in cockatiel flight direction were best explained by changes in roll orientation between wingbeats, which are not correlated with changes in roll within each wingbeat, and that are likely to be the combined result of both inertial and aerodynamic effects (Hedrick and Biewener, 2007). When compared with birds performing similar turns, bats produced tighter maneuvers, allowing them to complete the turn in a smaller number of wingbeats than pigeons and cockatiels (Warrick and Dial, 1998; Hedrick and Biewener, 2007). These differences could be the result of differences in size. *C. brachyotis* are approximately 10 times smaller in mass than cockatiels, and it has been suggested that maneuverability is inversely related to body size (Aldridge, 1987; Stockwell, 2001). Whether these differences in turning performance are a consequence of differences in size or due to differences in turning mechanisms is not known.

Studies of 180 deg. turns in microchiropteran bats have shown that bats initiate turns by flying upwards and decelerating (Rayner and Aldridge, 1985; Aldridge, 1987). We observed similar patterns in the present study, although our bats maintained their net forward speed throughout the recorded portion of the turn. The curvatures of the turns observed in our experiment were 3–23 times smaller (i.e. greater turning radius) than those observed for other bat species performing 180 deg. turns (Aldridge, 1987). Such variation is to be expected, considering the differences in task and body sizes.

The use of a combination of crabbed and banked mechanisms to produce a turn is likely to increase the maneuverability of bats compared with a mechanism that employs lift alone. The net influence of the crabbed component on turning is not readily quantified but it is clearly important for insects (Dudley, 2002). For example, in dragonflies capable of both banked and crabbed turns, the latter strategy produces turns at much higher rates, with changes in direction of 180 deg. in less than three wingbeats (Alexander, 1986). This degree of maneuverability is similar to that observed in the bats during the present study, where 180 deg. turns can be achieved in 3–4 wingbeats, although no information is available on whether the turn was banked, crabbed or a combination of both (Tian et al., 2006).

Our findings show that bats use a combination of crabbed and banked mechanisms to produce centripetal accelerations required to perform a turn. *C. brachyotis* changed its heading during upstroke and, thus, reoriented the body in such a way that the forward component of the net aerodynamic force produced during downstroke was aligned with the direction of travel. Therefore, the reorientation of the body and the bank angle of the body acts synergistically to produce a centripetal force. Bats seemed to actively change their yaw and pitch whereas changes in roll were compensatory to maintain a constant bank attitude. Reorientation during a wingbeat cycle is probably the result of the combination of aerodynamic and inertial forces, and future research should include estimation of how asymmetries in wingbeat kinematics to estimate the magnitude of inertial reorientation.

We thank Lubee Bat Conservancy and Dr Allyson Walsh for loaning us the bats; Andrew Biewener and the Harvard University Concord Field Station for allowing us the use of their facilities; Pedro Ramírez for caring for the bats; Kevin Middleton, Rachel Roemer, Allyce Sullivan, Ming-Ming Lee, Joe Wofford, Ann Atwood and Claudio Hetz for help with the experiments. We thank Ty Hedrick for his help during analysis and writing and David Willis for developing the mass model to estimate the CoM. Thanks to Daniel K. Riskin, Kenny Breuer, David Willis, Tatjana Hubel, Kristin Bishop and the Morphology group at Brown University for comments and discussions of the manuscript. Two anonymous reviewers provided particularly insightful comments on early drafts of this manuscript. This research was supported by the AFOSR, NSF-ITR and the Bushnell Foundation.

LIST OF ABBREVIATIONS

$\mathbf{A}_b$	acceleration vector of the body in the global coordinate system
$\mathbf{A}_{b,xy}$	acceleration vector of the body in the horizontal plane X_g–Y_g of the global coordinate system
$\mathbf{A}_{c,bank}$	estimated centripetal acceleration produced by the roll angle of the body
$\mathbf{A}_{c,total}$	centripetal acceleration necessary to produce a turn with a radius $1/\kappa$
$\mathbf{A}_{CoM,z}$	vertical acceleration of the CoM in the global coordinate system
CoM	center of mass
DLT	direct linear transformation
$\boldsymbol{g}$	acceleration of gravity
GLM	general lineal model
m_T	total mass of the bat
$\vec{r}_{CoM}$	position vector of the CoM
$\vec{r}_i$	position vector of the i-th discrete point mass
$\mathbf{V}_b$	velocity vector of the body in the global coordinate system
$\mathbf{V}_{b,xy}$	velocity vector of the body in the horizontal plane X_g–Y_g of the global coordinate system
$x_by_bz_b$	cartesian coordinates in the body-based coordinate system
$x_gy_gz_g$	cartesian coordinates in the global coordinate system
$X_bY_bZ_b$	dynamic, body-based coordinate system (centered on the hip)
$X_gY_gZ_g$	fixed, global coordinate system
γ_v, γ_h	vertical and horizontal stroke plane angle, respectively
κ	curvature in the horizontal plane X_g–Z_g
φ	bearing angle
ψ, θ, ϕ	heading, elevation and bank angle, respectively, in the global coordinate system

REFERENCES

Aldridge, H. (1986a). Manoeuvrability and ecological segregation in the little brown (*Myotis lucifugus*) and Yuma (*M. yumanensis*) bats (Chiroptera: Vespertilionidae). *Can. J. Zool.* **64**, 1878-1882.

Aldridge, H. D. (1986b). Kinematics and aerodynamics of the greater horseshoe bat, *Rhinolophus ferrumequinum*, in horizontal flight at various speeds. *J. Exp. Biol.* **126**, 479-497.

Aldridge, H. D. (1987). Turning flight of bats. *J. Exp. Biol.* **128**, 419-425.

Alexander, D. E. (1986). Wind tunnel studies of turns by flying dragonflies. *J. Exp. Biol.* **122**, 81-98.

Arabyan, A. and Tsai, D. (1998). A distributed control model for the air-righting reflex of a cat. *Biol. Cybern.* **79**, 393-401.

Berger, S. and Kutsch, W. (2003). Turning manoeuvres in free-flying locusts: high-speed video-monitoring. *J. Exp. Zool.* **299A**, 127-138.

Bishop, K. L. and Brim-DeForest, W. (2008). Kinematics of turning maneuvers in the Southern flying squirrel, *Glaucomys volans*. *J. Exp. Zool.* **309A**, 225-242.

Card, G. and Dickinson, M. (2008). Performance trade-offs in the flight initiation of *Drosophila*. *J. Exp. Biol.* **211**, 341-353.

Dudley, R. (2002). Mechanisms and implications of animal flight maneuverability. *Integr. Comp. Biol.* **42**, 135-140.

Filippone, A. (2006). *Flight Performance of Fixed and Rotary Wing Aircraft*. Oxford: Butterworth-Heinemann.

Fry, S. N., Sayaman, R. and Dickinson, M. H. (2003). The aerodynamics of free-flight maneuvers in *Drosophila*. *Science* **300**, 495-498.

Ghose, K. and Moss, C. F. (2003). The sonar beam pattern of a flying bat as it tracks tethered insects. *J. Acoust. Soc. Am.* **114**, 1120-1131.

Ghose, K. and Moss, C. F. (2006). Steering by hearing: a bat's acoustic gaze is linked to its flight motor output by a delayed, adaptive linear law. *J. Neurosci.* **26**, 1704-1710.

Ghose, K., Horiuchi, T. K., Krishnaprasad, P. S. and Moss, C. F. (2006). Echolocating bats use a nearly time-optimal strategy to intercept prey. *PLoS Biol.* **4**, e108.

Hatze, H. (1988). High-precision three-dimensional photogrammetric calibration and object space reconstruction using a modified DLT-approach. *J. Biomech.* **21**, 533-538.

Hedrick, T. L. (2007). DLTDataviewer2 for Matlab. (http://www.unc.edu/%7Ethedrick/software1.html).

Hedrick, T. L. and Biewener, A. A. (2007). Low speed maneuvering flight of the rose-breasted cockatoo (*Eolophus roseicapillus*). I. Kinematic and neuromuscular control of turning. *J. Exp. Biol.* **210**, 1897-1911.
Hedrick, T. L., Tobalske, B. W. and Biewener, A. A. (2002). Estimates of circulation and gait change based on a three-dimensional kinematic analysis of flight in cockatiels (*Nymphicus hollandicus*) and ringed turtle-doves (*Streptopelia risotia*). *J. Exp. Biol.* **205**, 1389-1409.
Hedrick, T. L., Usherwood, J. R. and Biewener, A. A. (2007). Low speed maneuvering flight of the rose-breasted cockatoo (*Eolophus roseicapillus*). II. Inertial and aerodynamic reorientation. *J. Exp. Biol.* **210**, 1912-1924.
Kalcounis, M. C. and Brigham, R. M. (1995). Intraspecific variation in wing loading affects habitat use by little brown bats (*Myotis lucifugus*). *Can. J. Zool.* **73**, 89-95.
Kirkpatrick, S. J. (1990). The moment of inertia of bird wings. *J. Exp. Biol.* **151**, 489-494.
McCay, M. G. (2001). Aerodynamic stability and maneuverability of the gliding frog *Polypedates dennysi*. *J. Exp. Biol.* **204**, 2817-2826.
Norberg, U. M. (1976). Some advanced flight manoeuvres of bats. *J. Exp. Biol.* **64**, 489-495.
Norberg, U. M. (1990). *Vertebrate Flight.* Berlin: Springer-Verlag.
Norberg, U. M. and Rayner, J. M. V. (1987). Ecological morphology and flight in bats (Mammalia; Chiroptera): wing adaptations, flight performance, foraging strategy and echolocation. *Philos. Trans. R. Soc. Lond., B, Biol. Sci.* **316**, 335-427.
Norberg, U. M. L. and Winter, Y. (2006). Wing beat kinematics of a nectar-feeding bat, *Glossophaga soricina*, flying at different flight speeds and Strouhal numbers. *J. Exp. Biol.* **209**, 3887-3897.
Phillips, W. F. (2004). *Mechanics of Flight.* Hoboken, NJ: Wiley.
Rayner, J. M. V. and Aldridge, H. D. (1985). Three-dimensional reconstruction of animal flight paths and the turning flight of microchiropteran bats. *J. Exp. Biol.* **118**, 247-265.
Spedding, G. R., Rosén, M. and Hedenström, A. (2003). A family of vortex wakes generated by a thrush nightingale in free flight in a wind tunnel over its entire natural range of flight speeds. *J. Exp. Biol.* **206**, 2313-2344.
Stockwell, E. F. (2001). Morphology and flight manoeuvrability in New World leaf-nosed bats (Chiroptera: Phyllostomidae). *J. Zool.* **254**, 505-514.
Swartz, S. M. (1997). Allometric patterning in the limb skeleton of bats: implications for the mechanics and energetics of powered flight. *J. Morph.* **234**, 277-294.
Swartz, S. M., Groves, M. D., Kim, H. D. and Walsh, W. R. (1996). Mechanical properties of bat wing membrane skin. *J. Zool.* **239**, 357-378.
Thollesson, M. and Norberg, U. M. (1991). Moments of inertia of bat wings and body. *J. Exp. Biol.* **158**, 19-35.
Tian, X., Iriarte-Díaz, J., Middleton, K., Galvao, R., Israeli, E., Roemer, A., Sullivan, A., Song, A., Swartz, S. and Breuer, K. (2006). Direct measurements of the kinematics and dynamics of bat flight. *Bioinspir. Biomim.* **1**, S10-S18.
Walker, J. A. (1998). Estimating velocities and accelerations of animal locomotion: a simulation experiment comparing numerical differentiation algorithms. *J. Exp. Biol.* **201**, 981-995.
Warrick, D. R. (1998). The turning- and linear-maneuvering performance of birds: the cost of efficiency for coursing insectivores. *Can. J. Zool.* **76**, 1063-1079.
Warrick, D. R. and Dial, K. P. (1998). Kinematic, aerodynamic and anatomical mechanisms in the slow, maneuvering flight of pigeons. *J. Exp. Biol.* **201**, 655-672.
Warrick, D. R., Dial, K. P. and Biewener, A. A. (1998). Asymmetrical force production in the maneuvering flight of pigeons. *Auk* **115**, 916-928.
Watts, P., Mitchell, E. J. and Swartz, S. M. (2001). A computational model for estimating the mechanics of horizontal flapping flight in bats: model description and validation. *J. Exp. Biol.* **204**, 2873-2898.
Woltring, H. J. (1986). A FORTRAN package for generalized, cross-validatory spline smoothing and differentiation. *Adv. Engng. Soft.* **8**, 104-113.
Yeadon, M. R. (1997). The biomechanics of the human in flight. *Am. J. Sports Med.* **25**, 575-580.